Porous Li-rich cathode material with modified surface by carbonaceous compounds for high performance lithium ion batteries with reduced voltage decay

Xin He,[a] Jun Wang,[a] Rui Wang,[b] Bao Qiu,[c] Henrich Frielinghaus*,[b] Philip Niehoff,[a] Haidong Liu,[a] Marian Cristian Stan,[a] Elie Paillard,[d] Martin Winter,[a] Jie Li*,[a]

[a] MEET Battery Research Center, Institute of Physical Chemistry, University of Muenster, Corrensstrasse 46, 48149 Muenster, Germany

[b] Jülich Centre for Neutron Science at MLZ, Forschungszentrum Jülich GmbH, Lichtenbergstrasse 1, D-85747 Garching, Germany

[c] Ningbo Institute of Materials Technology and Engineering (NIMTE), Chinese Academy of Sciences, Ningbo, Zhejiang, 315201, China

[d] Helmholtz Institute Münster – Forschungszentrum Jülich GmbH (IEK12), Corrensstraße 46, 48149 Münster, D-48149 Münster, Germany

KEYWORDS: lithium ion batteries, Li-rich cathode material; porous; carbonaceous compounds; cycling stability

ABSTRACT: High crystallinity Li-rich porous materials integrating with an in-situ formed surface containing carbonaceous compounds are synthesized through a facile approach. The rationally designed procedure involves the formation of a specific morphology of a hydroxide precursor assisted by a self-made template and subsequent high temperature treatment to obtain $Li_{1.2}Mn_{0.56}Ni_{0.16}Co_{0.08}O_2$ target product. The porous morphology is investigated using field-emission scanning electron microscopy and its surface area quantitatively examined by gas sorption analysis couple with the Brunauer-Emmett–Teller method. The crystallinity is characterized by X-ray diffraction and high-resolution transmission electron microscopy. X-ray photoelectron spectroscopy, CHN element analysis and small angle neutron scattering confirm the presence of the carbonaceous compounds in the surface composition. The prepared material exhibits superior discharge rate capability and excellent cycling stability. It shows minor capacity loss after 100 cycles at 0.5 C and maintains 94.9% of its initial capacity after 500 cycles at 2 C. Even more notably, the "voltage decay" during cycling is also significantly decreased. It has been found that carbonaceous compounds play a critical role for reducing the layered to spinel structural transformation during cycling. Therefore, the present porous Li-rich material with surface modified a carbonaceous compounds represents an attractive material for advanced Lithium-ion batteries.

1. Introduction

Li-rich layered oxides ($Li_{1+x}Mn_yTM_{1-x-y}O_2$, TM = Ni, Co, Fe, or Cr)[1] are considered as a most promising family of intercalation cathode materials for rechargeable lithium batteries, in particular lithium ion batteries (LIB)[2], owing to the advantages of high discharge capacity and high specific energy. Coupled with other benefits like high safety, low toxicity and costs, Li-rich metal oxides are currently significantly attractive for high-power applications, especially for hybrid electric vehicles.[3-5] However, weaknesses like intrinsic poor rate capability, dramatically decrease in the discharge potential plateau (so-called "voltage decay"), irreversible volume expansion and capacity fade during long-term cycling are bringing up concerns about their practical utilization, which need to be surmounted.[6-9]

Many efforts have been expended to overcome these issues. The controls of the particle size, crystallinity and structural morphology have obvious effects on electrochemical performance of electrode materials. For example, retaining the particle size within the nanometer scale is a feasible strategy for both anode[10] and cathode materials,[11] since smaller particles provide shorter diffusion pathways for lithium ions as well as faster electron transport, a higher electrode/electrolyte interface area and better accommodation of the strain of lithium intercalation/deintercalation, thus leading to improved rate performance.[12] Various nanostructured cathode materials have also been fabricated to improve the rate capability and cycling stability, such as hierarchical nanoplate,[11, 13] hollow spheres,[8, 14] mesoporous-macroporous materials.[15-17]

However, due to the high surface area, undesirable electrode/ electrolyte reactions occur in operation potential regions, which directly result in an enhancement of self-discharge, low Coulombic efficiency and poor cycling stability.[18] In addition, for the material synthesized through a conventional calcination route, a high crystallinity is usually incompatible with a small particle size and large specific surface area.[16] To achieve a combination of high crystallinity and large specific surface area, several specific morphologies have been developed for the cathode materials, in particular porous structures. Controlled design of a porous nano-structured architecture permits intimate penetration of the active material particle by the electrolyte.[19] Besides, a suitable pore size and a high porosity can also help to stabilize the dimensional integrity and buffer the irreversible volume expansion during cycling and is thus beneficial for the capacity retention during cycling[20] due to the reduced stress inside the particle agglomerate.

Though porous cathode materials in principal has the potential for an enhanced cycling performance, the rate performance can still be limited by the fact, that the pore-walls themselves are poorly electron conducting.[21] Consequently, surface modification with an electronically conducting agent can be expected to enhance the electrochemical performance of the active material. Extensive studies have been carried out on using carbon as a conductive coating or as additive filler to the electrode composite.[22-24] However, the traditional carbon coating methods is difficult to apply to the layered oxide cathode materials, since carbon tends to reduce the desired high valence state of transition metal ions during the high temperature calcination step and thus destroys the structure of the material.[25-28] Up to now there are only a few studies about carbon coating or carbon filler additives for electrodes using the Li-rich cathode material. Methods like synthesizing a carbon coating by a thermal evaporation technique[29, 30] or using carbon nano-fiber as electrode additive[31, 32] have been proven to improve rate capability and cycling stability of the Li-rich cathode material by forming an effective carbon surface film.

In this work, we introduce for the first time a facile synthesis approach a high crystallinity Li-rich material with large specific surface area and a surface modified with carbonaceous compounds resulting in a material with tailored porous architecture and a surface with better conductivity. The surface modified porous-structured Li-rich material is expected to yield improved rate capability when investigated as cathode material for LIBs. Furthermore, respectable cycling performance is also anticipated because of high crystallinity. A layered Li-rich material with the composition $Li_{1.2}Mn_{0.56}Ni_{0.16}Co_{0.08}O_2$ is used as an example to verify the validity of our hypothesis.

2. Experimental

Material synthesis. The preparation of the porous $Li_{1.2}Mn_{0.56}Ni_{0.16}Co_{0.08}O_2$ material (PS-LMNC) involves three key steps as illustrated by Scheme 1. First, the transition metal ions were co-precipitated with self-made polystyrene (PS) templates (details in the Supporting Information) by adding stoichiometric amounts of LiOH and NH_4OH solutions. 5.146 g $Mn(AC)_2{\cdot}4H_2O$, 1.493 g $Ni(AC)_2{\cdot}4H_2O$ and 0.747 g $Co(AC)_2{\cdot}4H_2O$ were dissolved in 100ml deionized water and stirred at room temperature for 20 min, then mixed with the PS precursor solution containing 70 ml ethanol as solvent. After stirring the mixture for 10 minutes, stoichiometric amounts of 1 mol/L LiOH and NH_4OH solutions were subsequently added under stirring at room temperature. The obtained $TM(OH)_2$ was precipitating on the PS to yield a well-encapsulating coating layer, thus forming new particles suspended in solution. Then the solution was heated under the Ar gas protection at 120 °C for 5 h to evaporate most of the water and the remaining powder was dried by freeze dryer (Christ Beta 2-4 LD Plus LT) at -104 °C, which resulted in a homogeneous black powder. The final product (PS-LMNC) was obtained by annealing the black powder at 800 °C for 20 hours. For comparison, a sample of the same composition was also prepared by a conventional co-precipitation method (CP-LMNC) without using any template, the conditions of the high temperature treatment were kept the same.[33]

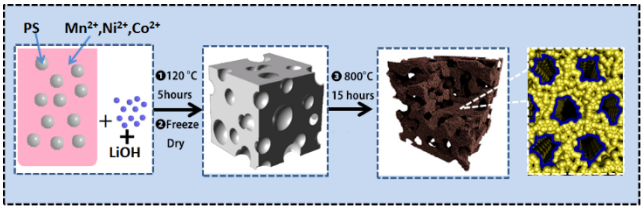

Scheme 1. Schematic illustration for the formation of porous $Li_{1.2}Mn_{0.56}Ni_{0.16}Co_{0.08}O_2$

Characterization. The crystal structure of the prepared materials was characterized by X-ray diffraction (XRD) on the Bruker D8 Advance (Bruker) diffractometer with Cu Kα radiation (1.54 Å) at room temperature. The pattern was recorded in the 2θ range of 15-90 ° at a scan rate of 0.00919 °/step and a count time per step of 5s. Rietveld refinement was taken to examine the effect of the transition metal ratio on the structure of PS-LMNC and CP-LMNC samples. The software TOPAS·Ver.·4.1·program was adopted to perform the refinement based on the R-3m and the C2/m structure modes. Particle morphology was evaluated using field-emission scanning electron microscopy (FE-SEM, Zeiss Auriga). The detailed crystal structure was further analyzed by transmission electron microscopy (TEM, Zeiss Libra 200 FE) operating at 200 kV. Selected area electron diffraction (SAED) patterns were recorded by a Gatan CCD camera in a digital format. The specific surface area was determined by the Brunauer-Emmett–Teller (BET) method by physisorption of nitrogen using the ASAP 2020 system (Micromeritics, Accelerated Surface Area and Porosimetry Analyzer). X-ray photoelectron spectroscopy (XPS, Axis Ultra HSA, Kratos, GB) was used to investigate the surface chemistry of the sample materials. The source energy was supported by a monochromatic Al Kα source (h·ν = 1486.6 eV), at a 10 mA filament current and a 12 kV filament voltage source energy. The analysis area was

approximately 700 µm × 300 µm. The carbon, nitrogen and hydrogen content in the composite was quantitatively determined by Vario EL III Element Analyzer ((Elementar Analysen System GmbH, Germany) through thermal decomposition at high temperature combustion in an oxygen-rich environment. The information on structure, shape, size and interactions of the component were characterized to a high precision via the KWS-1 Small-angle neutron scattering (SANS) instrument (of the Jülich Centre for Neutron Science at the research reactor FRM IIat the Heinz Maier-Leibnitz Zentrum in Garching) with a maximum neutron flux of ca. 1×10^{8} $cm^{-2}s^{-1}$. The 64 cm × 64 cm large area position-sensitive detector was moved within the 20m-long vacuum tube for optimal resolution. A neutron wavelength of 7 Å and collimation/detector distance of 20, 8 and 2 m were used to obtain the maximum structural information.[34] An impedance spectroscopy with Novocontrol AN-alpha analyzer and POT/GAL 20/11 electrochemical test station is employed to investigate the electronic conductivity. Both sample materials were pressed with a force of 117.6 kN cm^{-2} into 1.2 mm thick pellets. The diameter of each pellet is 13 mm. Before the conductivity measurement, both sides of each pellet was coated with 120 nm thick Au by sputter coating device. During the investigation process, an alternating current (frequency range from 100 mHz to 10 MHz) voltage of 1 V was utilized at room temperature.

Electrode preparation and cell assembly. The slurry to prepare the cathode electrodes was obtained by mixing the active materials, conductive carbon (Super C65, Timcal) and binder (polyvinylidene difluoride PVdF, Kynar® FLEX 2801, Arkema Group) in the weight ratio of 80:10:10, with N-methyl-2-pyrrolidone (NMP) as processing solvent. The well-mixed slurry was coated on an Al foil and dried at 80 °C overnight. After being punched into Ø 12 mm disc, the electrodes were further dried for 12 h under vacuum at 110 °C. The electrochemical performance was evaluated with 2032 coin cell system, using lithium metal as the counter electrode. The cathode electrode and lithium metal were separated by glass fiber (Whatman GF/D) wetted with electrolyte, which consisted of 1M $LiPF_6$ in ethylene carbonate (EC) and dimethyl carbonate (DMC) with a volume ratio of 1:1. Galvanostatic cycling tests were carried out on MACCOR series 4000 battery testers in a voltage range of 2.0–4.8 V at various current rates. All potentials reported in this work have been measured in a two-electrode cell configuration vs. Li metal.

3. Results and discussion

The morphologies of CP-LMNC and PS-LMNC (Figure 1) were firstly characterized by SEM. Figure 1a shows that the CP-LMNC powder contains aggregates of primary, spherically shaped particles. The primary particles, which can be clearly observed in Figure 1b, are homogeneous and have a size between 50 and 200 nm. Figure 1c gives an overview on the morphology of the PS-LMNC material, and it can be seen that the pores have been formed within the whole material, the vacancy is offered by the burning off of PS template. The porosity not only provides enough free volume for crystal growth,[13] but also facilitate the inter-diffusion of Li^{+} within the particles during charge and discharge process. In parallel, as illustrated by Figure 1d, the f PS-LMNC sample shows larger particle size and better crystallinity with single crystal particles rather than randomly agglomerate nanoparticles without defined edges (Figure 1b). In addition, the specific surface area for the PS-LMNC and CP-LMNC, as detected by the BET method, are 9.17 m^2 g^{-1} and 2.04 m^2 g^{-1}, respectively. The results clearly show that the surface area of PS-LMNC is dramatically larger than CP-LMNC. In other words, even without very distinct changes in particle size, the surface area as well as the electrode/electrolyte interface area of PS-LMNC particles is larger because of the higher porosity. The nitrogen adsorption/desorption isotherms shown in FigureS.1 indicate that the pore volume of PS-LMNC is much larger than that of CP-LMNC. The capillary condensation effect on PS-LMNC results in a hysteresis in the high p/p_o range, proving the porosity in the particles of the sample.[35] A high-resolution transmission electron microscopy (HRTEM) micrograph from a representative particle of the PS-LMNC sample is shown in Figure1e. The distance between two lattice fringes was calculated to be 0.471 nm, which can be indexed as $(003)_R$ planes from the rhombohedral (R) structure. Figure 1f shows single crystal electron diffraction pattern (EDP) from the corresponding particle, which is a clear evidence for the coexistence of $LiMO_2$ (M = Ni, Co, Mn) and Li_2MnO_3 domains.[36]

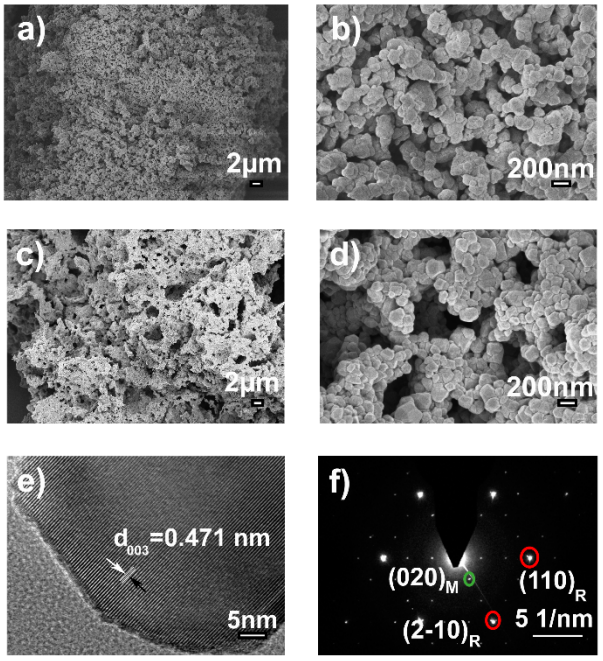

Figure 1. SEM images of (a, b) CP-LMNC and (c, d) PS-LMNC obtained at two different magnifications. (e) HRTEM image for PS-LMNC. (f) Electron diffraction pattern (EDP) from a particle of PS-LMNC.

Next, the two materials were characterized by XRD. Figure 2 displays the representative XRD patterns for the resulting $Li_{1.2}Mn_{0.56}Ni_{0.16}Co_{0.08}O_2$ materials (Figure 2 a & b) and the enlarged views of four different 2θ ranges (Figure

2 c-f). Different from other reports, that the spinel phase can be easily formed in the layered Li-rich material, when synthesis with an organic template,[27] there is no peaks assigned to the spinel-phase for our materials. In addition, an impure layered structure,[13] which may add shoulders next to the main diffraction peaks, in peculiarly the (003), (101), and (104) peaks, can also not be observed. These results indicate that a pure PS-LMNC phase was successfully achieved through a synthesis procedure involving a template- scarification in situ to the formation of the active phase. Compared to the CP-LMNC material, the PS-LMNC shows a narrow full width at half maxima (FWHM) in both, the (003) peak in Figure 2c and the (104) peak in Figure 2e. Both indicated that the material has better crystallinity, which is in good agreement with SEM images. In parallel, the PS-LMNC also exhibits a better split of the (018) and (110) peaks, demonstrating an improved layered structure. The integrated intensity ratio, I_{003}/I_{104}, of PS-LMNC (in the value of 1.23) is higher than that of CP-LMNC (in the value of 1.14) and with value higher than 1.2 indicates low cation mixing.[37] The lattice parameters of the LMNC materials obtained by structure refinement are summarized in Table S1. The contents of MNC phase for both materials are about 60 %, which indicates that the R-3m is the main phase. Thus, the layered structure property will be discussed with refinement data from this phase. The average metal-metal inter-slab distance is given by the parameter *c*. It is slightly increased for PS-LMNC compared with CP-LMNC. The trigonal distortion related with the *c*/*a* ratio, the higher *c*/*a* value from PS-LMNC indicates a better defined hexagonal layered structure for it.[38] It can be concluded that PS-LMNC has a higher degree of crystallinity and a higher fraction of the desired layered structure.

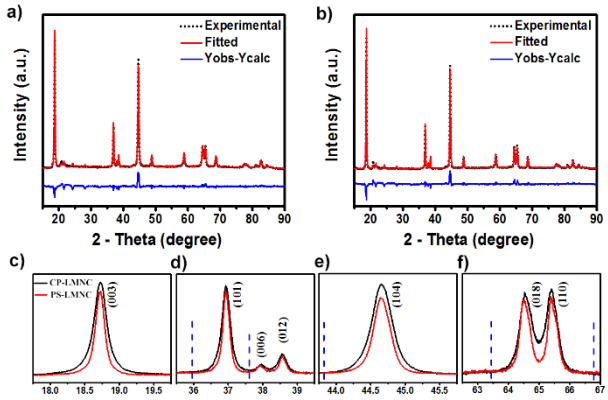

Figure 2. Powder X-ray diffraction patterns of (a) CP-LMNC; (b) PS-LMNC; and (c, d, e, f) local magnifications in the different 2θ ranges.

The surface s of the synthesized PS-LMNC and CP-LMNC samples were analyzed by X-ray photoelectron spectroscopy (XPS). The XPS spectra of C1s (a), O1s (b) and Mn2P (c) for both CP-LMNC and PS-LMNC powder are compared in Figure 3. The C1s spectrum of CP-LMNC shows the only peak at 284.5 eV, which corresponds to hydrocarbon contaminations.[39] The C1s spectrum of PS-LMNC can be fitted with six peaks which are located at 284.4, 285, 286, 286.8, 288.8 and 290.1 eV, respectively. The peaks at 284.4, 285 and 286 eV are assigned to sp^2 C-C, amorphous C-C bonds and the satellite peak of the sp^2 C-C group, respectively.[27, 40-42] The peaks at 286.8, 288.8 and 290.1 eV can be assigned to different carbon atom to oxygen bonds, including C-O, O-C=O and a carbon atom bond to a species with three oxygen. It can be assumed that layered (or surface modified) organic or lithium-poor semi alkyl carbonates ($ROCO_2Li$ or polymeric-type $ROCO_2R'$) are formed on the surface of the PS-LMNC. This assumption is supported by finding a broad peak at 532.7 eV in the O1s spectrum and a possible overlapping peak at 533.5 eV. These are the binding energies associated with the carbonyl-oxygen bonds and the oxygen bound to the alkyl group, respectively, however they cannot be clearly resolved.[39, 43, 44] Nevertheless, the peak representing organic or semi organic carbonates is not present in the CP-LMNC O1s spectrum. In addition, comparing the peak in the O1s spectrum at 529.5 eV, representing the LMNC metal oxide signal, it can be noticed that the signal is significantly lower for the PS-LMNC. This indicates that a significant surface film has been formed on PS-LMNC. Analogously, the peaks in the Mn2p spectrum of PS-LMNC sample are much lower compared to the ones of CP-LMNC. This confirms that the bulk material of PS-LMNC is effectively modified with carbonaceous compounds on the surface.

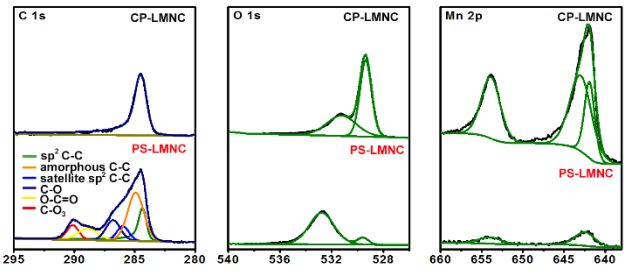

Figure 3. XPS spectra for C1s, O1s and Mn2p of the CP-LMNC and PS-LMNC materials.

The nanostructure and the surface coverage were also observed in complementary SANS experiments. Details of the used instrument KWS1 are described in Ref.[34]. The curves are described by 2 fractals using the model of Beaucage (Figure 4).[45] The dominant mass fractal arises from the LMNC particles, leading to a power law $d\Sigma/d\Omega = P \times Q^{-4}$ (Ω: solid angle of scattered neutrons; P: specific surface per volume of the particles; Q : scattering angle which is connected to the Fourier-Transformation of the real space structure (r→Q)), while the subtle deviation at $Q > 1.5$ nm^{-1} arises from the residual C/O surface coverage of the particles with a power law $d\Sigma/d\Omega = L \times Q^{-2}$ (L: specific surface coverage). The slight deviation of the exponent 3.8 in the case of the PS-LMNC sample was used for rescaling the bare Porod constant P. From P and an additional estimation of the particle concentration with respect to voids, the particle diameters of 150 and 250 nm are obtained for CP- LMNC and PS-LMNC, respectively, which is well in line with the SEM images. The off-leveling of the intensity at small $Q < 0.04$ nm^{-1} describes an effective correlation length of ca. 100 and 350 nm in

diameter and is obviously tightly connected to the hole size of the material (Figure 1). From the surface scattering, the ratio L/P can be determined to be δ = 0.69 for PS-LMNC and 0.88 nm for CP-LMNC, respectively. The slightly higher value can be assumed to appear due surface layer with a higher oxidation state, which means that less Li-rich component exists on the surface of the PS-LMNC sample. In parallel, the thickness of CP-LMNC and PS-LMNC is obtained to be d = 0.81 and 0.95 nm in the Guinier approximation. Both thicknesses d and δ agree reasonably well, since d corresponds to a real extension in space and δ is the compact equivalent. The systematically higher thickness of the surface layer for the PS-LMNC by 0.14 or 0.19 nm can be ratinlaized by the presence of ca. two atom layers of carbon, which derive from carbonaceous compounds, corresponding to the XPS analysis.

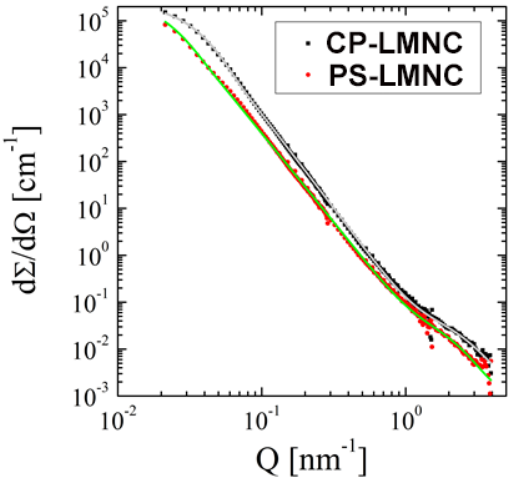

Figure 4. SANS curves for the powders CP-LMNC and PS-LMNC: Intensity as a function of the scattering vector Q. Fits were done with two fractal structures described by the Beaucage model.

The CHN analysis data (Table S2) confirms again the presence of carbon in PS-LMNC sample, the average carbon content is 0.2%, but no carbon can be detected in the CP-LMNC sample. Thought the carbon content is quite low, the positive effect is still expected on the electronic conductivity. In order to prove this, the solid electronic conductivity of the LMNC materials was measured by impedance spectroscopy at room temperature (Figure S2). The bulk electronic conductivity of PS-LMNC is 2.4×10^{-8} S cm^{-1}, and CP-LMNC is only 3.8×10^{-9} S cm^{-1}. Although high porosity in PS-LMNC sample can lead to an increased resistivity, the electronic conductivity of it is clearly higher than CP-LMNC. The measurement results show that the carbonaceous compounds can promote the electronic conductivity. As the matter of fact, the *in-situ* surface coating by carbonaceous compounds has a positive effect on the electrochemical performance, it can enhance charge transfer especially at high current density. Meanwhile, acting as efficient layer between the electrode and electrolyte, this carbonaceous surface can limit the side reaction of the electrolyte and maintain the structural stability of the active material, and as the result, facilitate the long term cycling behavior of the cell

To illustrate the advantage of the porous morphology with the carbon-based surface modification in the same material, the rate performance of the two Li-rich materials was compared. The discharge curves at different current densities, vary from 0.1 C to 10 C (1C=250 mA g^{-1}), are shown in Figure 5a. Both cells were cycled between 2.0-4.8 V. The PS-LMNC electrode shows better performance in specific capacity as well as rate capability. At a low discharge rate of 0.1 C, the CP-LMNC sample reaches a discharge capacity of ca. 250 mA g^{-1} while the PS-LMNC could achieve capacity above 270 mAh g^{-1}. Only 49.4 mAh g^{-1} of discharge capacity can be obtained with the CP-LMNC material at 10C, whereas PS-LMNC electrode still delivers 119.5 mAh g^{-1} at the same rate. It can be confirmed that the PS-LMNC shows very much improved high-rate capability, because the surface made from carbonaceous compounds provides an effective electron transport medium, while the porous structure offers the paths for rapid Li^+ insertion / extraction.

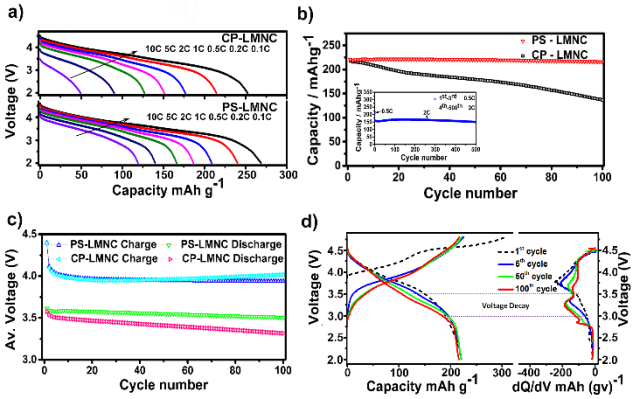

Figure 5. Comparison of (a) rate capabilities of CP-LMNC and PS-LMNC cathode materials at various rates, (b) cycling behavior of CP-LMNC and PS-LMNC at current rate of 0.5 C; inset shows the corresponding long term cycling performance of the PS-LMNC at 2 C after 3 formation cycles at 0.5 C, (c) average voltage as a function of cycle number for CP-LMNC and PS-LMNC, (d) voltage profiles and the corresponding discharge dQ/dV curves of the PS-LMNC sample at 0.5 C in the 1st, 5th, 50th and 100th cycles. All investigations were carried out between 2.0-4.8 V at 20 °C.

Considering that the layered Li-rich cathode always suffers from decomposition of the electrolyte and dissolution of transition-metal ions at high potential cycling,[46, 47] the in situ surface-modified material has the chance to reduce these detrimental effects during long term cycling. The cycling performance of the two materials were investigated at a current rate of 0.5 C (125 mAg^{-1}) and the results are shown in Figure 5b. The CP-LMNC sample delivers a capacity of 218 mAh g^{-1} in the first cycle at 0.5 C, but the discharge capacity abruptly decreases to 137 mAh g^{-1} after the 100th cycle, overall exhibiting a poor cycling stability. At contrast, the PS-LMNC can deliver a similar initial capacity and retains it in the test cycles with a minor loss 4.5 mAh g^{-1} (2.0 % of initial capacity). Even more excitingly, this very stable cycling performance can also be ob-

served at higher current rate of 2 C for 500 cycles, as being shown in the inset of Figure 5b. A reversible capacity of 150 mAh g^{-1} (ca. 94.9 % of the initial capacity) could be maintained after 500 cycles. It is common knowledge, that cycling at high rate will damage the layered structure and will lead to serious capacity fade.[46, 48, 49] In contrast, the PS-LMNC material shows excellent capacity retention, most probably due to the in situ formed carbonaceous surface compounds which protect the cathode material from reaction with the electrolyte.

From the point of view of practical application, in addition to the capacity, the voltage change during cycling is of great importance. From 1st to the 2nd cycle, a decrease of the charging voltage profile can be observed for the CP-LMNC and PS-LMNC materials. This can be explained as the effect of the irreversible structure change during the electrochemical activation of Li_2MnO_3-region happening in the initial cycle.[50, 51] Afterwards, the charging voltage profiles of the two materials perform differently from each other. Whereas, the voltage profile and the average voltage values of the PS-LMNC material keeps steady with negligible decrease, the CP-LMNC sample shows a clear increasing trend in voltage. The difference in the charging voltage reflects the difference in inner resistance. In other words, the PS-LMNC material demonstrates a lower inner resistance and better structural stability during cycling. We attribute the carbonaceous surface compounds confining the reaction with the electrolyte and the porous morphology buffering the volume change for the improved performance. The average discharge voltages tend to decrease for both materials, but the decay is much slower for the PS-LMNC material, with only 0.084 V of voltage decay after 100 cycles, while it is 0.34 V for the CP-LMNC material. The rapid decay of CP-LMNC reveals a faster layered-into-spinel phase transformation during cycling.[52] It can be assumed that the carbonaceous surface compounds in combination with the porous particle morphology can reduce the material phase change, and obviously decreases the voltage decay, as well. It is important to notice that to the best of our knowledge, the voltage decay exhibited by PS-LMNC material is one of the smallest reports so far.

Finally, Figure 5d displays the voltage profiles and the corresponding discharge dQ/dV curves of the PS-LMNC sample at the 1st, 5th, 50th and 100th cycle. The discharge profiles move to lower voltage plateaus in the first 50 cycles resulting in a minor loss of energy, but no voltage decay is found during prolonged cycling. Our synthesis method provides an effective method to address the problem for gradual layered-to-spinel transformation during cycling accompanied by capacity and voltage loss. It should be noted, that the layered-to-spinel transformation cannot be solved by adding carbon on the active material surface after synthesis.[32]

During the discharge, an obvious change happened at 3.5 V in the dQ/dV curve. A peak in the low voltage range which can be assigned to the Mn^{4+} / Mn^{3+} redox couple[53] appears and increases in intensity during cycling, while the peak in the high voltage range which belongs to the Ni^{4+} / Ni^{2+} and $Co^{3.6+}$ / Co^{3+} redox couples[53, 54] decreases continuously. Nevertheless, this change is less pronounced than in other literature reports. The PS-LMNC can deliver a discharge capacity of 106.4 mAh g^{-1} from 4.8 V to 3.5 V, indicating a good reversibility of the Ni^{4+} / Ni^{2+} and $Co^{3.6+}$ / Co^{3+} redox couples. Since Ni^{4+} / Ni^{2+} and $Co^{3.6+}$ / Co^{3+} are from the $LiMO_2$ region, this is a proof for the high stability of the R-3m layered structure. Even though the layered-to-spinel phase transformation during discharge still exists, it is obviously suppressed by the good crystallinity of the material and the surface modification with carbonaceous compounds. As a result, the PS-LMNC material achieves excellent energy retention (Figure 5c).

4. Conclusions

Outstanding rate and long-term cycling performance of PS-LMNC material can be achieved by a reasonable material design by a sophisticated synthesis approach. The material structure and composition combines a tailored porosity with a surface modified by carbonaceous compounds which results in reduced volume change, high Li+ ion conductivity and a good structural stability during Li+ insertion / extraction. The designed porous structure can achieve a balance between high crystallinity and large specific surface area. The outer carbonaceous compounds does not only increase electronic conductivity, but also form a protective surface coating in case of reaction of the electrolyte. The good compatibility of the surface modified with carbonaceous compounds and the layered Li-rich cathode material structure below reduces the detrimental layered-to-spinel transformation as well as the voltage decay. These findings prove the importance of the control and design of the cathode/electrolyte interface for reducing capacity fade and voltage decay of Li-rich cathode materials. This material is a large step to advanced LIBs with high voltage and high energy.

AUTHOR INFORMATION

Corresponding Author

Dr. Jie Li
Tel.: +49 251 8336702, Fax: +49 251 8336032
E-mail address: jie.li@uni-muenster.de
Dr. Henrich Frielinghaus
Tel.: +49 89 28910706, Fax: +49 89 28910799
E-mail address: h.frielinghaus@fz-juelich.de

ACKNOWLEDGMENT

The authors kindly acknowledge the financial support of Federal Ministry of Education and Research (*BMBF*), Federal Ministry of Economic and Technology and Federal Ministry for the Environment (*BMWi*), Nature Conservation and Nuclear Safety (*BMU*) of Germany within the project KaLiPat (03EK3008).

ABBREVIATIONS

PS-LMNC, porous $Li_{1.2}Mn_{0.56}Ni_{0.16}Co_{0.08}O_2$ material; CP-LMNC, co-precipitation method prepared $Li_{1.2}Mn_{0.56}Ni_{0.16}Co_{0.08}O_2$ material; PS, polystyrene; XRD, X-ray diffraction; XPS, X-ray photoelectron spectroscopy; FE-SEM, field-emission scanning electron microscopy; HRTEM, high-

resolution transmission electron microscopy; EDP, electron diffraction pattern; SAED, selected area electron diffraction; SANS, small-angle neutron scattering; PVdF, polyvinylidene difluoride; NMP, N-methyl-2-pyrrolidone; EC, ethylene carbonate; DMC, dimethyl carbonate.

SUPPORTING INFORMATION

Experimental process to prepare the monodispersed polystyrene template. The lattice parameters of CP-LMNC and PS-LMNC materials obtained by Rietveld refinement (Table S1). CHN-Analysis results for PS-LMNC and CP-LMNC materials (Table S2). Nitrogen adsorption-desorption isotherms of CP-LMNC and PS-LMNC materials (Figure S1). Plots of the conductivity vs. frequency for CP-LMNC and PS-LMNC materials (Figure S2). The information is available free of charge via the Internet at http://pubs.acs.org/.

REFERENCES

1. Thackeray, M. M.; Johnson, C. S.; Vaughey, J. T.; Li, N.; Hackney, S. A., Advances in manganese-oxide 'composite' electrodes for lithium-ion batteries. *Journal of Materials Chemistry* **2005,** 15, (23), 2257-2267.
2. Wagner, R.; Preschitschek, N.; Passerini, S.; Leker, J.; Winter, M., Current research trends and prospects among the various materials and designs used in lithium-based batteries. *Journal of Applied Electrochemistry* **2013,** 43, (5), 481-496.
3. Kang, S. H.; Kempgens, P.; Greenbaum, S.; Kropf, A. J.; Amine, K.; Thackeray, M. M., Interpreting the structural and electrochemical complexity of $0.5Li_2MnO_3\square0.5LiMO_2$ electrodes for lithium batteries (M = $Mn_{0.5-x}Ni_{0.5-x}Co_{2x}$, $0\leq x \leq 0.5$). *Journal of Materials Chemistry* **2007,** 17, (20), 2069-2077.
4. He, P.; Yu, H.; Li, D.; Zhou, H., Layered lithium transition metal oxide cathodes towards high energy lithium-ion batteries. *Journal of Materials Chemistry* **2012,** 22, (9), 3680-3695.
5. Yu, H.; Ishikawa, R.; So, Y.-G.; Shibata, N.; Kudo, T.; Zhou, H.; Ikuhara, Y., Direct Atomic-Resolution Observation of Two Phases in the $Li_{1.2}Mn_{0.567}Ni_{0.166}Co_{0.067}O_2$ Cathode Material for Lithium-Ion Batteries. *Angewandte Chemie International Edition* **2013,** 52, (23), 5969-5973.
6. Liu, H.; Qian, D.; Verde, M. G.; Zhang, M.; Baggetto, L.; An, K.; Chen, Y.; Carroll, K. J.; Lau, D.; Chi, M.; Veith, G. M.; Meng, Y. S., Understanding the Role of NH4F and Al2O3 Surface Co-modification on Lithium-Excess Layered Oxide $Li_{1.2}Ni_{0.2}Mn_{0.6}O_2$. *Acs Applied Materials & Interfaces* **2015,** 7, (34), 19189-19200.
7. Liu, H.; Fell, C. R.; An, K.; Cai, L.; Meng, Y. S., In-situ neutron diffraction study of the $xLi_2MnO_3\cdot(1-x)LiMO_2$ ($x = 0, 0.5$; M = Ni, Mn, Co) layered oxide compounds during electrochemical cycling. *Journal of Power Sources* **2013,** 240, 772-778.
8. He, X.; Wang, J.; Kloepsch, R.; Krueger, S.; Jia, H.; Liu, H.; Vortmann, B.; Li, J., Enhanced electrochemical performance in lithium ion batteries of a hollow spherical lithium-rich cathode material synthesized by a molten salt method. *Nano Research* **2014,** 7, (1), 110-118.
9. Wang, J.; He, X.; Kloepsch, R.; Wang, S.; Hoffmann, B.; Jeong, S.; Yang, Y.; Li, J., Increased Capacity of $LiNi_{1/3}Co_{1/3}Mn_{1/3}O_2$–$Li[Li_{1/3}Mn_{2/3}]O_2$ Cathodes by MnOx-surface Modification for Lithium-Ion Batteries. *Energy Technology* **2014,** 2, (2), 188-193.
10. Besenhard, J. O.; Wachtler, M.; Winter, M.; Andreaus, R.; Rom, I.; Sitte, W., Kinetics of Li insertion into polycrystalline and nanocrystalline `SnSb' alloys investigated by transient and steady state techniques. *Journal of Power Sources* **1999,** 81–82, (0), 268-272.
11. Wei, G.-Z.; Lu, X.; Ke, F.-S.; Huang, L.; Li, J.-T.; Wang, Z.-X.; Zhou, Z.-Y.; Sun, S.-G., Crystal Habit-Tuned Nanoplate Material of $Li[Li_{1/3-2x/3}Ni_xMn_{2/3-x/3}]O_2$ for High-Rate Performance Lithium-Ion Batteries. *Advanced Materials* **2010,** 22, (39), 4364-4367.
12. Shaju, K. M.; Bruce, P. G., A Stoichiometric Nano-$LiMn_2O_4$ Spinel Electrode Exhibiting High Power and Stable Cycling. *Chemistry of Materials* **2008,** 20, (17), 5557-5562.
13. Chen, L.; Su, Y.; Chen, S.; Li, N.; Bao, L.; Li, W.; Wang, Z.; Wang, M.; Wu, F., Hierarchical $Li_{1.2}Ni_{0.2}Mn_{0.6}O_2$ Nanoplates with Exposed {010} Planes as High-Performance Cathode Material for Lithium-Ion Batteries. *Advanced Materials* **2014,** 26, (39), 6756-6760.
14. Jiang, Y.; Yang, Z.; Luo, W.; Hu, X.; Huang, Y., Hollow $0.3Li_2MnO_3\square0.7LiNi_{0.5}Mn_{0.5}O_2$ microspheres as a high-performance cathode material for lithium-ion batteries. *Physical Chemistry Chemical Physics* **2013,** 15, (8), 2954-2960.
15. Qu, Q.; Fu, L.; Zhan, X.; Samuelis, D.; Maier, J.; Li, L.; Tian, S.; Li, Z.; Wu, Y., Porous $LiMn_2O_4$ as cathode material with high power and excellent cycling for aqueous rechargeable lithium batteries. *Energy & Environmental Science* **2011,** 4, (10), 3985-3990.
16. Huang, Z.-D.; Liu, X.-M.; Oh, S.-W.; Zhang, B.; Ma, P.-C.; Kim, J.-K., Microscopically porous, interconnected single crystal $LiNi_{1/3}Co_{1/3}Mn_{1/3}O_2$ cathode material for Lithium ion batteries. *Journal of Materials Chemistry* **2011,** 21, (29), 10777-10784.
17. Ren, Y.; Armstrong, A. R.; Jiao, F.; Bruce, P. G., Influence of Size on the Rate of Mesoporous Electrodes for Lithium Batteries. *Journal of the American Chemical Society* **2009,** 132, (3), 996-1004.
18. Arico, A. S.; Bruce, P.; Scrosati, B.; Tarascon, J.-M.; van Schalkwijk, W., Nanostructured materials for advanced energy conversion and storage devices. *Nat Mater* **2005,** 4, (5), 366-377.
19. Jiao, F.; Shaju, K. M.; Bruce, P. G., Synthesis of Nanowire and Mesoporous Low-Temperature $LiCoO_2$ by a Post-Templating Reaction. *Angewandte Chemie International Edition* **2005,** 44, (40), 6550-6553.
20. Ge, M.; Rong, J.; Fang, X.; Zhou, C., Porous Doped Silicon Nanowires for Lithium Ion Battery Anode with Long Cycle Life. *Nano Letters* **2012,** 12, (5), 2318-2323.
21. Guo, Y.-G.; Hu, J.-S.; Wan, L.-J., Nanostructured Materials for Electrochemical Energy Conversion and Storage Devices. *Advanced Materials* **2008,** 20, (15), 2878-2887.
22. Qi, X.; Blizanac, B.; DuPasquier, A.; Lal, A.; Niehoff, P.; Placke, T.; Oljaca, M.; Li, J.; Winter, M., Influence of Thermal Treated Carbon Black Conductive Additive on the Performance of High Voltage Spinel Cr-

Doped $LiNi_{0.5}Mn_{1.5}O_4$ Composite Cathode Electrode. *Journal of The Electrochemical Society* **2015,** 162, (3), A339-A343.
23. Qi, X.; Blizanac, B.; DuPasquier, A.; Meister, P.; Placke, T.; Oljaca, M.; Li, J.; Winter, M., Investigation of PF6- and TFSI- anion intercalation into graphitized carbon blacks and its influence on high voltage lithium ion batteries. *Physical Chemistry Chemical Physics* **2014,** 16, (46), 25306-25313.
24. Qi, X.; Blizanac, B.; DuPasquier, A.; Oljaca, M.; Li, J.; Winter, M., Understanding the influence of conductive carbon additives surface area on the rate performance of $LiFePO_4$ cathodes for lithium ion batteries. *Carbon* **2013,** 64, (0), 334-340.
25. Cao, Q.; Zhang, H. P.; Wang, G. J.; Xia, Q.; Wu, Y. P.; Wu, H. Q., A novel carbon-coated $LiCoO_2$ as cathode material for lithium ion battery. *Electrochemistry Communications* **2007,** 9, (5), 1228-1232.
26. Kim, H.-S.; Kong, M.; Kim, K.; Kim, I.-J.; Gu, H.-B., Effect of carbon coating on $LiNi_{1/3}Mn_{1/3}Co_{1/3}O_2$ cathode material for lithium secondary batteries. *Journal of Power Sources* **2007,** 171, (2), 917-921.
27. Guo, R.; Shi, P.; Cheng, X.; Du, C., Synthesis and characterization of carbon-coated $LiNi_{1/3}Co_{1/3}Mn_{1/3}O_2$ cathode material prepared by polyvinyl alcohol pyrolysis route. *Journal of Alloys and Compounds* **2009,** 473, (1–2), 53-59.
28. Goodenough, J. B.; Kim, Y., Challenges for Rechargeable Li Batteries†. *Chemistry of Materials* **2009,** 22, (3), 587-603.
29. Shi, S. J.; Tu, J. P.; Mai, Y. J.; Zhang, Y. Q.; Gu, C. D.; Wang, X. L., Effect of carbon coating on electrochemical performance of $Li_{1.048}Mn_{0.381}Ni_{0.286}Co_{0.286}O_2$ cathode material for lithium-ion batteries. *Electrochimica Acta* **2012,** 63, (0), 112-117.
30. Liu, J.; Wang, Q.; Reeja-Jayan, B.; Manthiram, A., Carbon-coated high capacity layered $Li[Li_{0.2}Mn_{0.54}Ni_{0.13}Co_{0.13}]O_2$ cathodes. *Electrochemistry Communications* **2010,** 12, (6), 750-753.
31. Martha, S. K.; Nanda, J.; Veith, G. M.; Dudney, N. J., Electrochemical and rate performance study of high-voltage lithium-rich composition: $Li_{1.2}Mn_{0.525}Ni_{0.175}Co_{0.}1O_2$. *Journal of Power Sources* **2012,** 199, (0), 220-226.
32. Martha, S. K.; Nanda, J.; Veith, G. M.; Dudney, N. J., Surface studies of high voltage lithium rich composition: $Li_{1.2}Mn_{0.525}Ni_{0.175}Co_{0.1}O_2$. *Journal of Power Sources* **2012,** 216, (0), 179-186.
33. Li, J.; Kloepsch, R.; Stan, M. C.; Nowak, S.; Kunze, M.; Winter, M.; Passerini, S., Synthesis and electrochemical performance of the high voltage cathode material $Li[Li_{0.2}Mn_{0.56}Ni_{0.16}Co_{0.08}]O_2$ with improved rate capability. *Journal of Power Sources* **2011,** 196, (10), 4821-4825.
34. Feoktystov, A. V.; Frielinghaus, H.; Di, Z.; Jaksch, S.; Pipich, V.; Appavou, M.-S.; Babcock, E.; Hanslik, R.; Engels, R.; Kemmerling, G.; Kleines, H.; Ioffe, A.; Richter, D.; Brückel, T., KWS-1 high-resolution small-angle neutron scattering instrument at JCNS: current state. *Journal of Applied Crystallography* **2015,** 48, (1), 61-70.
35. Shi, S. J.; Tu, J. P.; Tang, Y. Y.; Zhang, Y. Q.; Wang, X. L.; Gu, C. D., Preparation and characterization of macroporous $Li_{1.2}Mn_{0.54}Ni_{0.13}Co_{0.13}O_2$ cathode material for lithium-ion batteries via aerogel template. *Journal of Power Sources* **2013,** 240, (0), 140-148.
36. Yu, X.; Lyu, Y.; Gu, L.; Wu, H.; Bak, S.-M.; Zhou, Y.; Amine, K.; Ehrlich, S. N.; Li, H.; Nam, K.-W.; Yang, X.-Q., Understanding the Rate Capability of High-Energy-Density Li-Rich Layered $Li_{1.2}Ni_{0.15}Co_{0.1}Mn_{0.55}O_2$ Cathode Materials. *Advanced Energy Materials* **2014,** 4, (5), n/a-n/a.
37. Idemoto, Y.; Matsui, T., Thermodynamic stability, crystal structure, and cathodic performance of $Lix(Mn_{1/3}Co_{1/3}Ni_{1/3})O_2$ depend on the synthetic process and Li content. *Solid State Ionics* **2008,** 179, (17–18), 625-635.
38. Deng, C.; Zhang, S.; Wu, B.; Yang, S. Y.; Li, H. Q., Synthesis and characteristics of nanostructured $Li(Co_{1/3}Ni_{1/3}Mn_{1/3})O_2$ cathode material prepared at 0 °C. *Journal of Solid State Electrochemistry* **2010,** 14, (5), 871-875.
39. Andersson, A. M.; Abraham, D. P.; Haasch, R.; MacLaren, S.; Liu, J.; Amine, K., Surface Characterization of Electrodes from High Power Lithium-Ion Batteries. *Journal of The Electrochemical Society* **2002,** 149, (10), A1358-A1369.
40. Patsalas, P.; Handrea, M.; Logothetidis, S.; Gioti, M.; Kennou, S.; Kautek, W., A complementary study of bonding and electronic structure of amorphous carbon films by electron spectroscopy and optical techniques. *Diamond and Related Materials* **2001,** 10, (3-7), 960-964.
41. Mérel, P.; Tabbal, M.; Chaker, M.; Moisa, S.; Margot, J., Direct evaluation of the sp3 content in diamond-like-carbon films by XPS. *Applied Surface Science* **1998,** 136, (1-2), 105-110.
42. Edström, K.; Gustafsson, T.; Thomas, J. O., The cathode–electrolyte interface in the Li-ion battery. *Electrochimica Acta* **2004,** 50, (2–3), 397-403.
43. Haik, O.; Leifer, N.; Samuk-Fromovich, Z.; Zinigrad, E.; Markovsky, B.; Larush, L.; Goffer, Y.; Goobes, G.; Aurbach, D., On the surface chemistry of $LiMO_2$ cathode materials (M= [MnNi] and [MnNiCo]): Electrochemical, spectroscopic, and calorimetric studies. *Journal of The Electrochemical Society* **2010,** 157, (10), A1099-A1107.
44. Kerber, S. J.; Bruckner, J. J.; Wozniak, K.; Seal, S.; Hardcastle, S.; Barr, T. L., The nature of hydrogen in x-ray photoelectron spectroscopy: General patterns from hydroxides to hydrogen bonding. *Journal of Vacuum Science & Technology A* **1996,** 14, (3), 1314-1320.
45. Beaucage, G., Small-Angle Scattering from Polymeric Mass Fractals of Arbitrary Mass-Fractal Dimension. *Journal of Applied Crystallography* **1996,** 29, (2), 134-146.
46. Xu, B.; Fell, C. R.; Chi, M.; Meng, Y. S., Identifying surface structural changes in layered Li-excess nickel manganese oxides in high voltage lithium ion batteries: A joint experimental and theoretical study. *Energy & Environmental Science* **2011,** 4, (6), 2223-2233.
47. Sun, Y.-K.; Lee, M.-J.; Yoon, C. S.; Hassoun, J.; Amine, K.; Scrosati, B., The Role of AlF_3 Coatings in Improving Electrochemical Cycling of Li-Enriched Nickel-Manganese Oxide Electrodes for Li-Ion Batteries. *Advanced Materials* **2012,** 24, (9), 1192-1196.
48. Johnson, C. S.; Kim, J. S.; Lefief, C.; Li, N.; Vaughey, J. T.; Thackeray, M. M., The significance of the Li_2MnO_3 component in 'composite' xLi2MnO3□(1-x)$LiMn_{0.5}Ni_{0.5}O_2$ electrodes. *Electrochemistry Communications* **2004,** 6, (10), 1085-1091.
49. Thackeray, M. M.; Kang, S.-H.; Johnson, C. S.; Vaughey, J. T.; Benedek, R.; Hackney, S. A., Li_2MnO_3-stabilized $LiMO_2$ (M = Mn, Ni, Co) electrodes for lithium-ion batteries. *Journal of Materials Chemistry* **2007,** 17, (30), 3112-3125.
50. Mohanty, D.; Kalnaus, S.; Meisner, R. A.; Rhodes, K. J.; Li, J.; Payzant, E. A.; Wood Iii, D. L.; Daniel, C.,

Structural transformation of a lithium-rich $Li_{1.2}Co_{0.1}Mn_{0.55}Ni_{0.15}O_2$ cathode during high voltage cycling resolved by in situ X-ray diffraction. *Journal of Power Sources* **2013,** 229, (0), 239-248.

51. Rana, J.; Kloepsch, R.; Li, J.; Scherb, T.; Schumacher, G.; Winter, M.; Banhart, J., On the structural integrity and electrochemical activity of a $0.5Li_2MnO_3\square0.5LiCoO_2$ cathode material for lithium-ion batteries. *Journal of Materials Chemistry A* **2014,** 2, (24), 9099-9110.

52. Bettge, M.; Li, Y.; Gallagher, K.; Zhu, Y.; Wu, Q.; Lu, W.; Bloom, I.; Abraham, D. P., Voltage Fade of Layered Oxides: Its Measurement and Impact on Energy Density. *Journal of The Electrochemical Society* **2013,** 160, (11), A2046-A2055.

53. Lu, Z.; Dahn, J. R., Understanding the Anomalous Capacity of $Li/Li[Ni_xLi_{(1/3-2x/3)}Mn_{(2/3}\square_{-x/3)}]O_2$ Cells Using In Situ X-Ray Diffraction and Electrochemical Studies. *Journal of The Electrochemical Society* **2002,** 149, (7), A815-A822.

54. Song, B.; Liu, Z.; Lai, M. O.; Lu, L., Structural evolution and the capacity fade mechanism upon long-term cycling in Li-rich cathode material. *Physical Chemistry Chemical Physics* **2012,** 14, (37), 12875-12883.